Myoferlin targeting triggers mitophagy and primes ferroptosis in pancreatic cancer cells

Gilles Rademaker [a,2,1], Yasmine Boumahd [a,b,1], Raphaël Peiffer [a,b], Sandy Anania [a,b], Tom Wissocq [a], Maude Liégeois [c], Géraldine Luis [d], Nor Eddine Sounni [d], Ferman Agirman [a], Naïma Maloujahmoum [a], Pascal De Tullio [e], Marc Thiry [f], Akeila Bellahcène [a], Vincent Castronovo [a], Olivier Peulen [a,b,*]

[a] *Metastasis Research Laboratory, GIGA-cancer, University of Liège, Pathology Institute B23, B-4000, Liège, Belgium*
[b] *Center for Interdisciplinary Research on Medicines (CIRM), Mitochondria Adaptation in Cancer Group, University of Liège, B-4000, Liège, Belgium*
[c] *Laboratory of Cellular and Molecular Immunology, GIGA Institute, University of Liège, B-4000, Liège, Belgium*
[d] *Laboratory of Tumor and Development Biology, GIGA-cancer, University of Liège, Pathology Institute B23, B-4000, Liège, Belgium*
[e] *Center for Interdisciplinary Research on Medicines (CIRM), Metabolomics Group, University of Liège, B-4000, Liège, Belgium*
[f] *Laboratory of Cellular and Tissular Biology, GIGA-Neurosciences, Cell Biology L3, University of Liège, B-4000, Liège, Belgium*

A R T I C L E   I N F O

A B S T R A C T

Myoferlin, an emerging oncoprotein, has been associated with a low survival in several cancer types including pancreas ductal adenocarcinoma where it controls mitochondria structure and respiratory functions. Owing to the high susceptibility of KRAS-mutated cancer cells to iron-dependent cell death, ferroptosis, and to the high iron content in mitochondria, we investigated the relation existing between mitochondrial integrity and iron-dependent cell death. We discovered that myoferlin targeting with WJ460 pharmacological compound triggered mitophagy and ROS accumulation culminating with lipid peroxidation and apoptosis-independent cell death. WJ460 caused a reduction of the abundance of ferroptosis core regulators x_c^- cystine/glutamate transporter and GPX-4. Mitophagy inhibitor Mdivi1 and iron chelators inhibited the myoferlin-related ROS production and restored cell growth. Additionally, we reported a synergic effect between ferroptosis inducers, erastin and RSL3, and WJ460.

1. Introduction

Myoferlin is a recently identified oncoprotein involved in cell membrane biology and overexpressed in several cancers, including pancreatic ductal adenocarcinoma (PDAC) [1], where its expression is significantly correlated with poor patient outcome [2,3]. Previously, we demonstrated in PDAC cells that myoferlin is essential to several membrane events including exocytosis [4], and exosome function [5]. We also showed that it contributes to the regulation of the lipid metabolism, where it confers energetic flexibility [6]. More recently, we reported that myoferlin contributes significantly to the mitochondrial fitness in pancreas and colon cancer cells [3,7], probably through its interaction with mitochondrial dynamic machinery [8]. Recently, the contribution of mitochondria to cancer development and progression has become

firmly established [9], and our recent studies indicate that myoferlin could be a valuable target for new therapeutic strategies. This aspect appears increasingly pertinent as pharmacological compounds targeting myoferlin were recently described [10–12].

Recently, a specific iron-dependent form of programmed cell death, ferroptosis, was identified [13]. Interestingly, the x_c^- cystine/glutamate transporter, identified as a central element in this mechanism, was previously demonstrated as a mediator of PDAC growth with a role in drug resistance [14]. Deletion of the x_c^- system in KPC mice induced tumor ferroptosis and extended survival [15]. However, conditional depletion of x_c^- system from pancreatic epithelial cells in KPC mice did not lead to survival benefit suggesting the importance to target x_c^- system simultaneously in cancer and stromal compartments [16]. Additionally, report showed that cysteine starvation alone is not sufficient to induce

ferroptosis in pancreatic cancer [17].

Our study uncovers that myoferlin pharmacological targeting elicited a mitochondrial energetic stress in PDAC cell lines and triggered mitophagy culminating with ferroptosis.

2. Material and methods

2.1. Cells and chemicals

Human pancreatic cancer cells BxPC-3, Panc-1, MiaPaCa-2, and human pancreatic normal epithelial cells (HPNE) were purchased from ATCC (Manassas, VA). PaTu 8988T cell line was purchased from DSMZ (Braunschweig, Germany). WJ460 was obtained from Probechem (Shanghai, China). RSL3, erastin, deferiprone, deferoxamine were purchased from Sigma-Aldrich (Bornem, Belgium). Trolox was purchased from (TargetMol, Boston, MA, USA). Deuterium oxide (99.96%) and trimethylsilyl-3-propionic acid-d4 were purchased from Eurisotop (St-Aubin, France). The list of antibodies used is available as supplemental information.

2.2. Cell culture

BxPC-3, Panc-1, PaTu 8988T, MiaPaCa-2 cells were cultured as previously reported [3]. HPNE cells were cultured according to manufacturer recommendations. Cells were checked monthly for mycoplasma and used between passage 1 and 10. Except when mentioned otherwise, cell lines were seeded in 96-well plates (10^4 cells/well), or 6-well plates (3.10^5 cells/well) and treated with WJ460 for 8–48 h.

2.3. siRNA transfection and shRNA plasmid transduction

Cells were transfected with 20 nM siRNA (Eurogentec, Seraing, Belgium — siRNA#1 CCCUGUCUGGAAUGAGAUUT; siRNA#2 GAAA-GAGCUGUGCAUUAUAAA; irrelevant siRNA CUUACGCUGAGUA-CUUCGAT) using calcium phosphate as previously described [3].

ShRNA plasmid was transduced using lentiviral vectors in the GIGA institute viral vector facility. The sequence of myoferlin shRNA#1 corresponded to myoferlin siRNA#1.

2.4. Western-blot

Cells were lysed in 1% sodium dodecyl sulfate added with protease and phosphatase inhibitors. Western blots were performed as described previously [3].

2.5. Nuclear magnetic resonance-based targeted metabolomics

Cell pellets were suspended in 300 μl of D2O phosphate buffer (pH7.4), placed in a 2 ml centrifugation vial in an ice bath and then subjected to sonication with the vibrating probe (Vibra-Cell, Sonics & Materials Inc., Newtown, CT) for periods of 60s according to a described procedure [18]. The mixture was centrifuged (12 000 g, 5min, 4 °C) and the supernatant were collected and added with 10 μl of 3-(trimethylsilyl) propionic acid (TMSP). The solution was distributed into 3-mm tubes. The NMR spectra were recorded as previously described on a spectrometer Bruker Neo (Billerica, MA) [18]. The ratio oxidized glutathione (GSSG)/reduced glutathione (GSH) were obtained by integrations of the signals at 4,55 ppm and 2.93 ppm respectively using the following formula: GSSG/GSH = (integral at 2.93ppm-2*integral at 4.55 ppm)/(integral at 4.55 ppm*2). The obtained values were then corrected according to the number of cells.

2.6. Immunofluorescence

Cells were seeded on sterile glass coverslips and allowed to attach overnight. They were then treated with either vehicle or WJ460 for 24 h then ice-cold methanol/acetone (4:1) fixed. Cells were then blocked with 1% BSA for 30min and incubated overnight with primary antibody. Images were acquired using Nikon A1R confocal microscope.

2.7. Electronic microscopy

WJ460-treated cells were detached, washed with DPBS solution and fixed with 2.5% glutaraldehyde solution for 3 h at room temperature. After fixation cells were kept in Sorensen buffer, post-fixed for 60min in 2% osmium tetroxide. Observations were made with a Jeol (Tokyo, Japan) JEM-1400 transmission electron microscope at 80 kV.

2.8. Proliferation assay

PDAC cells were treated with different concentrations of WJ460, RSL3, erastin, deferiprone or deferoxamine and directly imaged with Incucyte S3 (Sartorius, Ann Arbor, MA). Confluency was then quantified using Incucyte analysis software.

2.9. Seahorse extracellular flux analysis

Experiments were performed with a XFp extracellular flux analyzer (Agilent, Santa Clara, CA). Cells (10^4 per well) were seeded and allowed to attach overnight. Cells were then treated with WJ460 or vehicle for 24 h. Seahorse experiments were performed as described previously [3]. Results were normalized according to cell number evaluated by Hoechst incorporation.

2.10. Mitochondrial footprint and mitophagy staining

Mitochondrial network integrity was assessed in live cells after 1 nM TMRE staining during 15min. Mitochondrial footprint, branch counts per network and branch length mean were evaluated using MiNA plugin for ImageJ. Mitophagy was detected in live cells after 50 nM WJ460 treatment (16 h–24 h) of mitophagy dye-loaded cells according to manufacturer instruction (Mitophagy detection kit, Dojindo Laboratories, Kumamoto, Japan). Cells were imaged using a Nikon A1R confocal microscope and integrated fluorescent intensities were quantified individually in each cell thanks to ImageJ.

2.11. Free iron determination

Intracellular iron concentration was estimated using FerroOrange dye according to manufacturer recommendations (Dojindo Laboratories, Kumamoto, Japan). Image acquisition and quantification were performed using Incucyte SX5 (Sartorius, Ann Arbor, MA).

2.12. Crystal violet staining

PDAC cells treated with WJ460 for 24 h were ice-cold methanol/acetone (4:1) fixed and incubated in a crystal violet solution for 20min.

2.13. Malondialdehyde assay

Malondialdehyde (MDA) was measured with MDA quantification kit (MAK085, Sigma-Aldrich). According to manufacturer's recommendations. Results were normalized to the number of cells.

2.14. Cell cycle analysis

Cell cycle of WJ460-treated cells was analyzed as previously described [7].

2.15. Reactive oxygen species determination

Total reactive oxygen species (ROS) production was measured by

flow cytometry using H2DCFDA (ThermoFischer Scientific, Waltham, MA) fluorescent probe according to the manufacturer's recommendations. Mitochondrial ROS were evaluated by confocal microscopy after staining with a singlet oxygen specific dye according to manufacturer instructions (Si-DMA, Dojindo Laboratories, Kumamoto, Japan).

2.16. Transferrin receptor flow cytometry

The membrane expression of CD71 was assessed with flow cytometry. Briefly, cells were stained for 30min with anti-human CD71 in presence of 5% FC Block (BD Biosciences). Cells were analyzed with a BD FACS Canto (BD Biosciences).

2.17. Ethics and animal experiments

All animal experimental procedures were performed according to the Federation of European Laboratory Animal Sciences Associations (FELASA) and were accepted after reviewing by the Institutional Animal Care and Ethics Committee of the University of Liège, Belgium (#2271). Animals were housed in the animal facility of the GIGA institute.

Panc-1 cells (10^6 cells – parental or myoferlin shRNA) were suspended in 100 μl DMEM and injected in the flank of 5-week-old NOD-SCID mice randomly assigned to experimental group. When tumors were palpable (day 7), WJ460 (10 mg/kg body weight) was daily injected intraperitoneally. WJ460 dose was selected according to Zhang et al. [10]. Tumor size was measured weekly during 4 weeks from the initiation of WJ460 treatment. During the 3 first weeks, tumor main axis were measured through the skin with a caliper and tumor volume was calculated according to ellipsoid formula ($v = 1/6 \times pi \times axis_1 \times axis_2 \times axis_3$). At week 4, tumors were resected and imaged. Tumor area was measured with imageJ then multiplied by thickness to obtain tumor volume. Each experiment was performed as 3 biological replicates. Sample size was chosen thanks to an a priori T-test power evaluation (software G-Power 3.1) using a 40% tumor volume reduction and 95% power.

2.18. Statistical analysis

All results were reported as means with standard error of the mean (SEM). Two-sided statistical analyses were performed. Unless mentioned otherwise, group means were compared by unpaired Student's T-test or Bonferroni's pairwise comparison according to the group number. Welsch's correction was applied when homoscedasticity was suspected. All experiments were performed as several independent biological replicates. Statistics were performed using Prism 5.0f. Survival analysis and cohort comparison were performed on cBioportal [19,20]. Synergy between WJ460 and RSL3 or Erastin was evaluated according to Chou-Talalay's methods [21] and using CompuSyn software (Chou TC and Martin N. CompuSyn for Drug Combinations, ComboSyn Inc, Paramus, NJ, 2005. www.combosyn.com).

3. Results

3.1. Pharmacological targeting of myoferlin mimicks myoferlin gene silencing

WJ460 was recently described and applied to breast cancer models [10]. Expecting to exploit this small molecule in PDAC, we initiate to reproduce the main effects raised by myoferlin siRNA transfection in PDAC cell lines. First, we decided to quantify PDAC cell confluency during 48 h in presence of WJ460 concentrations ranging from 1 to 100 nM (Fig. 1A). Relative confluency quantifications after 24 h WJ460 exposure showed that MiaPaCa-2 were the most sensitive to WJ460 (IC50 = 20.92 ± 1.02 nM) while BxPC-3 were the most resistant (IC50–48.44 nM) (Fig. 1B). Panc-1 (IC50 = 23.08 ± 1.08 nM) and PaTu 8988T (IC50–27.48 nM) presented an intermediate behavior.

Based on these results, we selected 50 nM WJ460 as the smallest common effective concentration. Undoubtedly, PDAC cells suffered from 50 nM WJ460 exposition as demonstrated by the decrease of cell number and by the increased number of rounded cells (Supplemental Fig. S1A). Interestingly, WJ460 did not alter normal pancreatic ductal epithelial cells (HPNE) growth (Fig. 1C). Then we used 50 nM WJ460 to validate the three main hallmarks of myoferlin silencing [3], namely loss of mitochondrial network integrity, decrease of oxygen consumption rate (OCR), and cytosolic reactive oxygen species (ROS) production. All PDAC cell lines suffered from a disintegration of the mitochondrial network when submitted to 50 nM WJ460 during 24 h while HPNE mitochondrial network was unaltered (Fig. 1D & Supplemental Fig. S1B). The extent of the mitochondrial network disorganization was in accordance with the IC50. BxPC-3 harbored a more preserved network than the 3 other cell lines. We next measured OCR in PDAC cell lines after 24 h WJ460 exposition. Globally mitochondrial respiration was significantly decreased in all tested cell lines (Fig. 1E) except HPNE (Fig. 1F). The main altered respiratory compartments were the basal OCR, ATP-production related OCR and maximal OCR (Supplemental Fig. S1C). Then we evaluated the ROS production 24 h after WJ460 exposition. The total ROS production was significantly increased in MiaPaCa-2, Panc-1 and PaTu 8988T but not in BxPC-3 and HPNE (Fig. 1G). Taken together these data indicate that 50 nM WJ460 during 24 h induces similar effects on PDAC cell lines to the ones we previously described upon myoferlin gene silencing [3]. Moreover, WJ460 injection in immunocompromised mice harboring pre-implanted Panc-1 tumors reduced significantly the tumor growth to a level similar to what was observed when myoferlin-depleted Panc-1 cells were grafted (Fig. 1H).
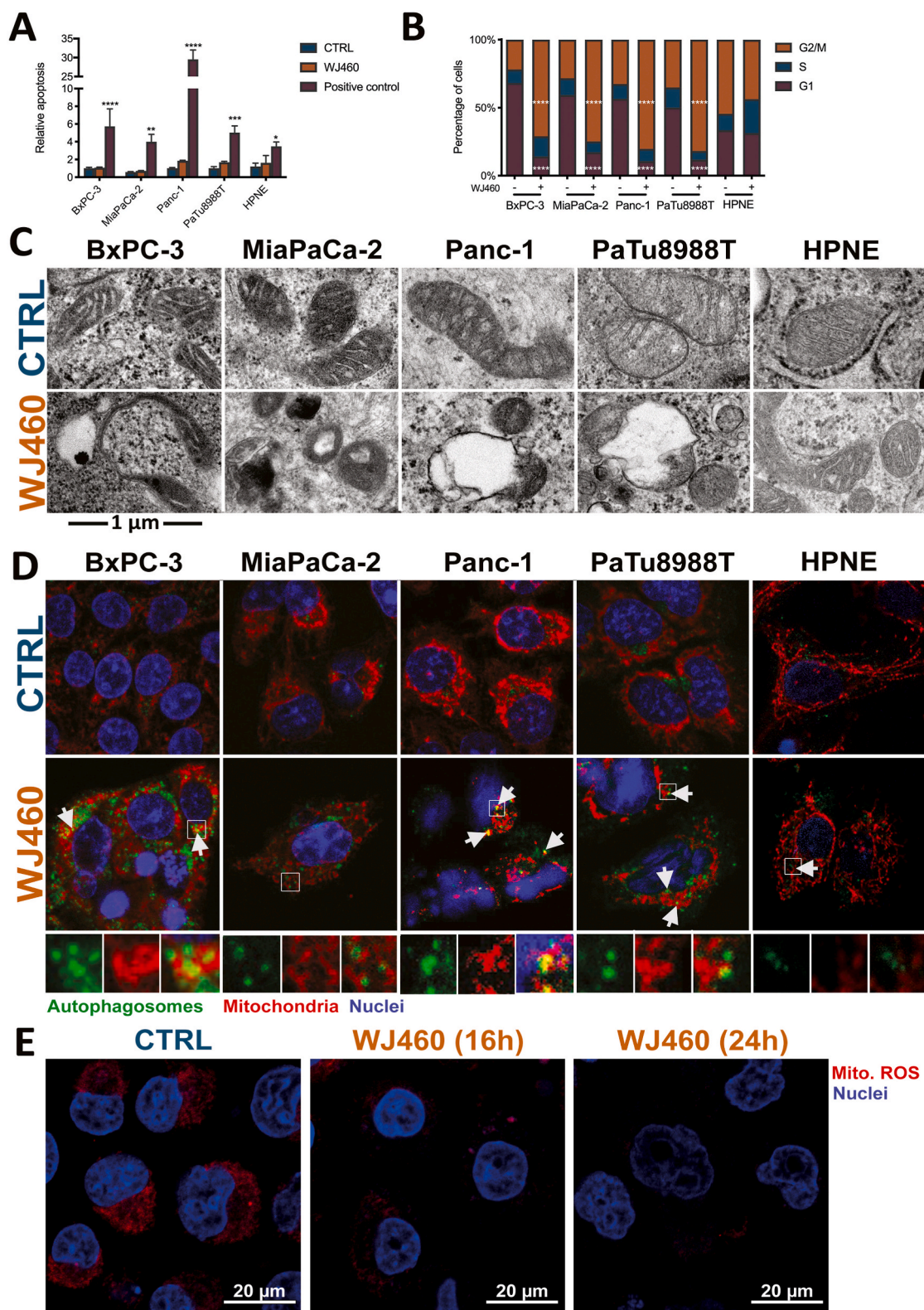
3.2. WJ460 triggers a cell cycle arrest in G2/M phase and mitophagy

Considering our finding, we then evaluated the potential contribution of apoptosis to the reduction of cell numbers. Cell culture were submitted to 50 nM WJ460 during 24 h and stained with FITC-conjugated annexin-V. Proportion of annexin-V positive cells was not significantly increased by WJ460 (Fig. 2A). Searching for the causes of the observed reduction of cell number, we decided to investigate the cell cycle. It appeared that, except in HPNE cells, pharmacological targeting of myoferlin completely reversed the G1/G2 ratio, indicating a G2/M blockade (Fig. 2B). While interesting, these results neither explained the rounding of the cells nor the decrease of their number. We thus undertook an ultrastructural analysis focusing our attention on mitochondria. While these organelles presented an expected morphology in the case of untreated cells, and in WJ460-treated HPNE, this was not the case in WJ460-treated PDAC cells. Indeed, a significant number of mitochondria were characterized by a disorganization of their cristae, by the appearance of empty areas, or even by their engulfment (Fig. 2C & Supplemental Fig. S2A). In MiaPaCa-2, mitochondria remained unaltered but in close vicinity to lysosomes. Similar observations were performed when myoferlin was silenced with siRNA (Supplemental Fig. S2B). We hypothesized that WJ460 triggered mitophagy. In order to test this hypothesis, we immunolocalized autophagosomes and mitochondria. Consistent with our hypothesis, the number of autophagosomes were increased in WJ460-treated cancer cells and several colocalization spots were identified in BxPC-3, Panc-1 and PaTu 8988T cell lines (Fig. 2D). In order to confirm this observation, we took advantage of a mitophagy detection kit using mitophagy-specific and lysosome-specific dyes (Supplemental Fig. S2C). We reported a significant increase of mitophagy-associated fluorescence in WJ460-treated cells. Accordingly, lysosomal-staining was also increased and colocalized with mitochondria. To support this discovery, we evaluated mitochondrial ROS reported to be decreased during mitophagy in PDAC [22]. Accordingly, our analysis revealed a significant decrease in mitochondrial ROS abundance in Panc-1 cells 16 h and 24 h after 50 nM WJ460 treatment (Fig. 2E).
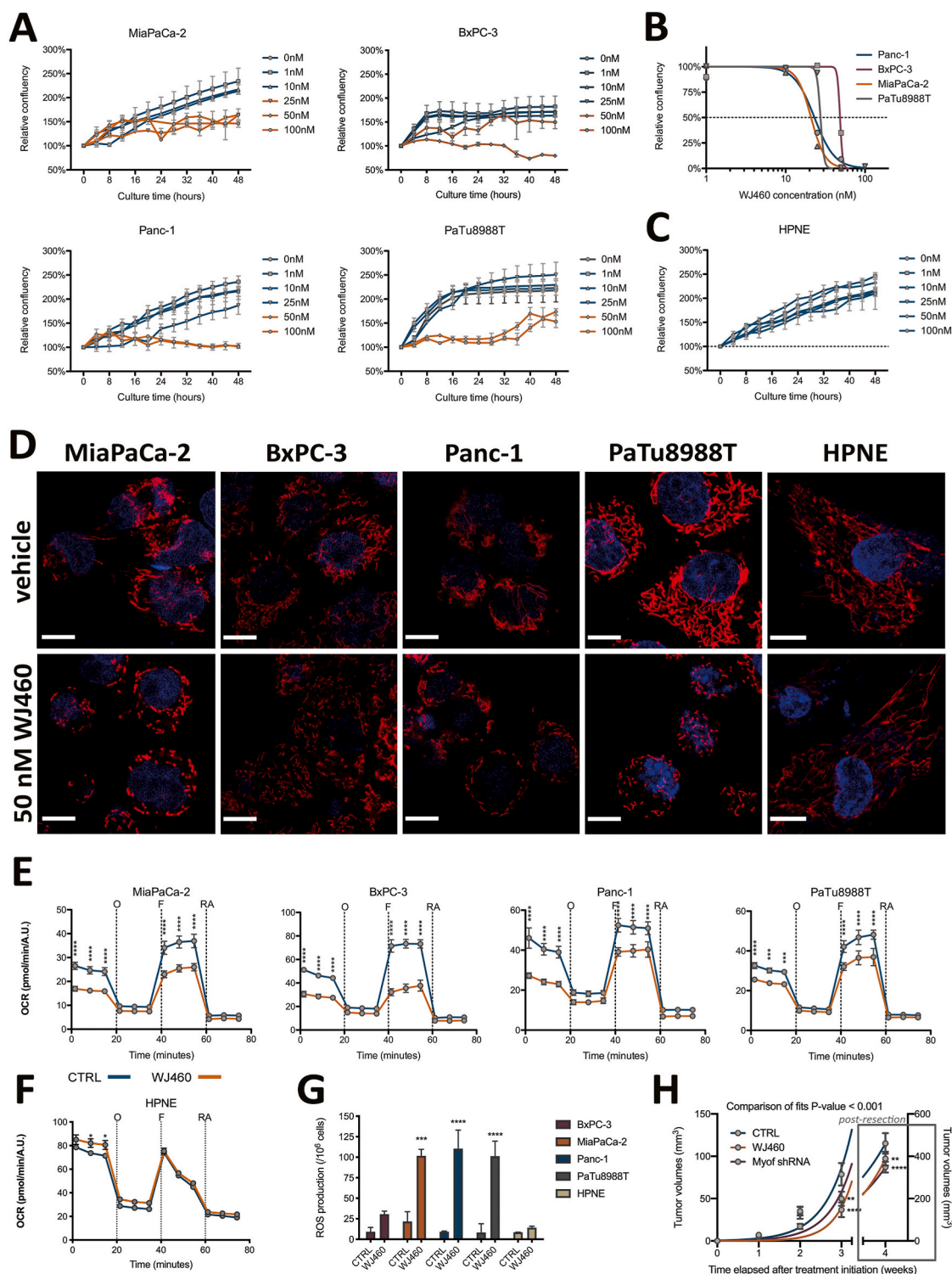
Fig. 1. Pharmacological targeting of myoferlin exhibits the same effects than myoferlin gene silencing.

(A) Treatment of PDAC cell lines (MiaPaCa-2, BxPC-3, Panc-1 and PaTu 8988T) with WJ460 ranging from 1 to 100 nM for the indicated times causes cell growth reduction. (B) WJ460 half maximal inhibitory concentration (IC50) determination in PDAC cell lines after 24 h exposition. (C) Treatment of pancreas normal epithelial cell line (HPNE) with WJ460 ranging from 1 to 100 nM for the indicated times. (D) Visualization of mitochondrial network shape of PDAC cell lines after 50 nM WJ460 treatment during 24 h. Scale bar = 10 μm, except for HPNE where scale bar = 7.5 μm. (E–F) Oxygen consumption rate (OCR) in PDAC cell lines and HPNE after 50 nM WJ460 treatment for 24 h. Kinetic oxygen consumption rate response of PDAC cells to 1 μM oligomycin (O), 1 μM FCCP (F), rotenone and antimycin A mix (RA, 0.5 μM each). Cell number was estimated using Hoechst incorporation (arbitrary unit, A.U.). Each data point represents mean ± SEM, n = 3. ****$P < 0.0001$, ***$P < 0.001$, *$P < 0.05$. (G) Reactive oxygen species (ROS) accumulation in PDAC cell lines and HPNE treated for 24 h with 50 nM WJ460. Each data point represents mean ± SEM, n = 3. ****$P < 0.0001$, ***$P < 0.001$. (H) Kinetic of Panc-1 cell tumor development in NOD-SCID mice upon WJ460 administration (10 mg/kg daily). ****$P < 0.0001$, **$P < 0.01$.

Fig. 2. WJ460 triggers a cell cycle arrest in G2/M phase and mitophagy in PDAC cell lines.
(A) Relative apoptosis measured by annexin-V staining in PDAC cell lines (BxPC-3, MiaPaCa-2, Panc-1 and PaTu 8988T) and HPNE treated for 24 h with 50 nM WJ460. Puromycin was used as a positive control. Each data point represents mean ± SEM, n = 5. ****P < 0.0001, ***P < 0.001, **P < 0.01, *P < 0.05. (B) Proportion of PDAC cells in each cell cycle phase was measured 24 h after 50 nM WJ460 treatment. Each data point represents mean ± SEM, n = 3. ****P < 0.0001. (C) Ultrastructure of mitochondria in PDAC cell lines treated for 24 h with 50 nM WJ460. (D) Immunofluorescence of autophagosome (LC3-II – green) and mitochondria (mitochondrial-specific 60 kDa protein - red) in PDAC cell lines and HPNE treated for 24 h with 50 nM WJ460. Arrows point to autophagosome and mitochondria colocalization. (E) Decrease of mitochondrial reactive oxygen species (Mito. ROS) accumulation in Panc-1 cell lines treated for 16 h or 24 h with 50 nM WJ460. (For interpretation of the references to colour in this figure legend, the reader is referred to the Web version of this article.)
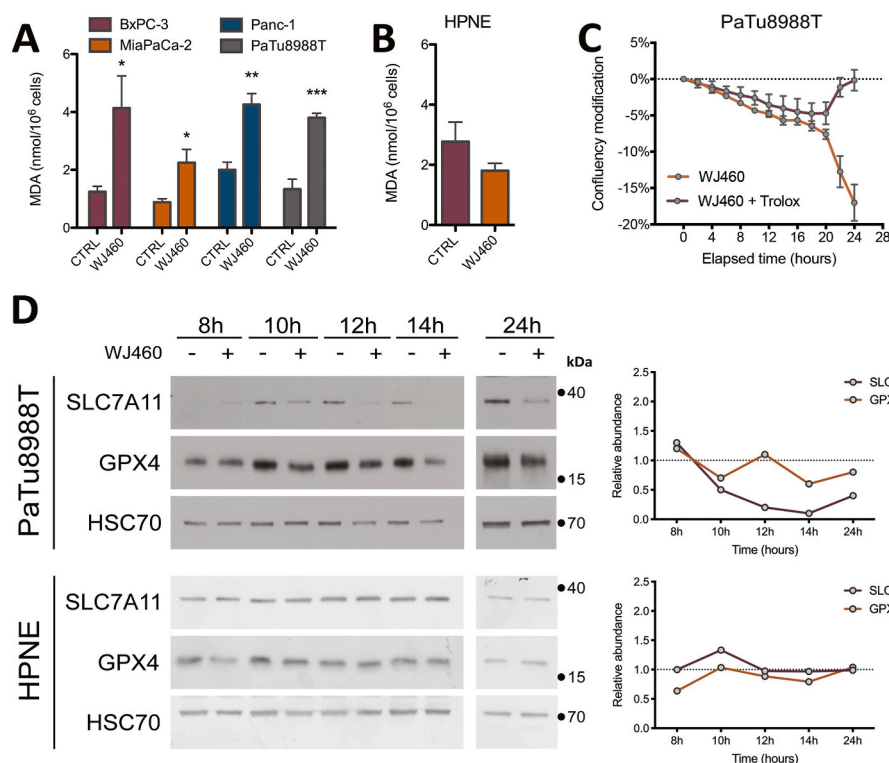
3.3. WJ460 promotes lipid peroxidation

Aware of the importance of mitochondria in ferroptosis [23], and considering the increase of ROS production upon WJ460 stimulation, we decided to investigate lipid peroxidation, a main hallmark of ferroptosis. Malondialdehyde concentration, resulting from lipid peroxidation, were significantly increased by 2- to 3-fold by 50 nM WJ460 (Fig. 3A). As a validation, we evaluated the same parameter after myoferlin silencing in Panc-1 cells, and a similar range of increase was observed (Supplemental Fig. S3A). Interestingly, HPNE cells had a basal MDA concentration similar to the one observed in untreated PDAC cells. However, WJ460 did not increase this concentration (Fig. 3B). In order to confirm the ferroptotic nature of the cell death, we performed a rescue experiment using Trolox, a vitamin E analog. PDAC cell lines were simultaneously treated with 50 nM WJ460 and 5 mM Trolox. The Trolox concentration was chosen based on a concentration-response experiment (Supplemental Fig. S3B). The kinetic of WJ460-induced modification of cell confluency was significantly reduced in all PDAC cell lines except in MiaPaCa-2 cell line (Fig. 3C & Supplemental Fig. S3C). We then sought to evaluate the redox status of the cells by analyzing the ratio of oxidized glutathione (GSSG) to reduced glutathione (GSH) by targeted metabolomics. This ratio was increased by 50% when Panc-1 cells were exposed for 24 h to 50 nM WJ460 (Supplemental Fig. S3D). Encouraged by these results we decided to analyze the abundance of the main ferroptosis core regulators: SLC7A11, a constituent of the x_c^- transporter, and glutathione peroxidase (GPX)-4, involved in the reduction of lipid peroxides. Our results showed a significant reduction of the abundance of these proteins when PDAC cells were treated for 8–24 h with 50 nM WJ460 (Fig. 3D & Supplemental Fig. S4A), indicating that cancer cells indeed suffered from a ROS imbalance and inactivated the common rescue pathways commonly altered in ferroptosis. Gene expression analysis, extracted from RNAseq dataset (Supplemental Fig. S4B) and confirmed by RTqPCR (Supplemental Fig. S4C), indicated a significant reduction of GPX4 gene expression upon WJ460 treatment while SLC7A11 gene expression was remained unchanged. Interestingly, and in accordance with the above observations, WJ460 altered neither

SLC7A11 nor GPX-4 abundance in HPNE cells (Fig. 3D). Additionally, we noticed a faint increase of SLC7A11 and GPX-4 abundance upon culture time in untreated PDAC cell lines but not in HPNE. This observation could be the result of a progressive nutrient-deprivation [24] occurring more rapidly in PDAC cell lines than in HPNE.
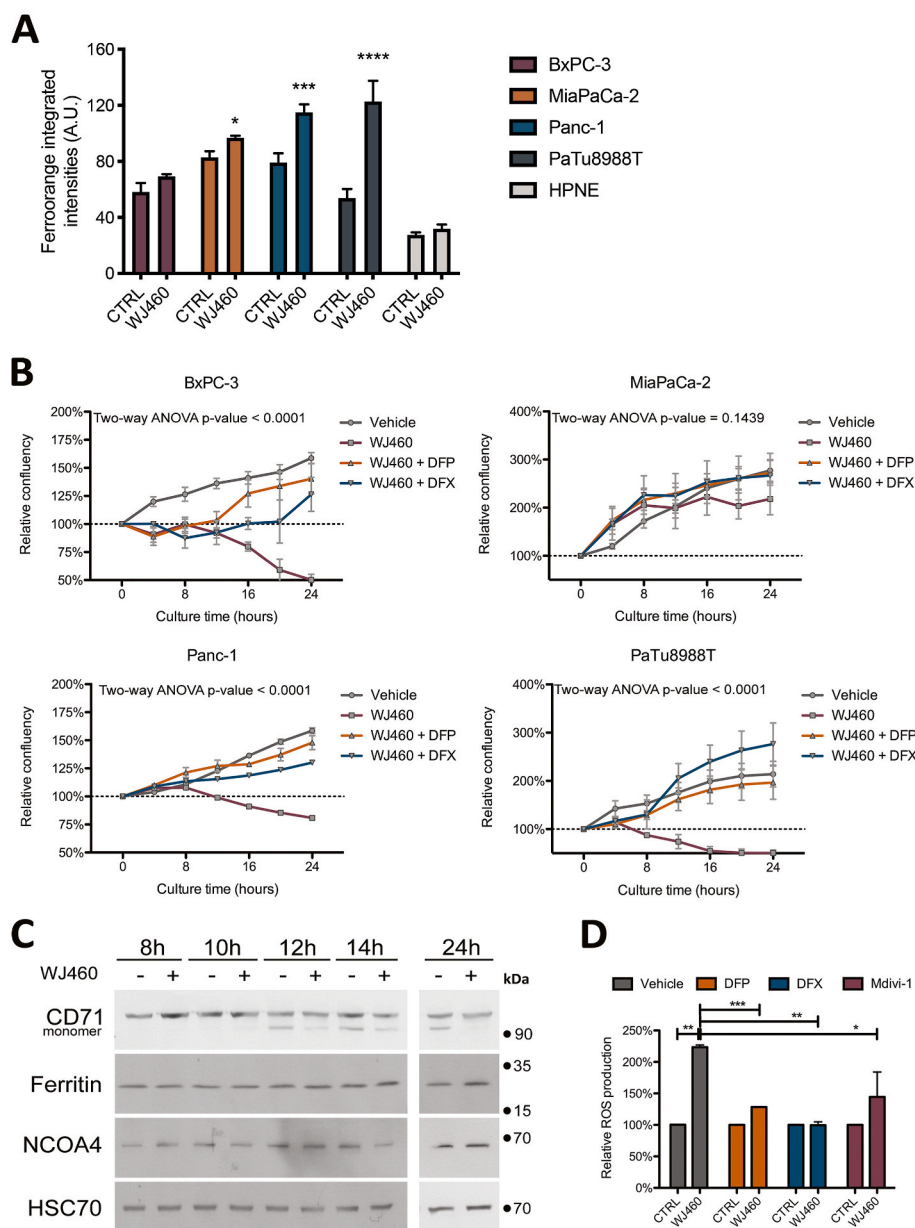
3.4. WJ460 triggers an iron-dependent cell death

In order to demonstrate an iron dependence in the cell growth reduction by WJ460, we estimated intracellular iron concentration 8 h, 16 h and 24 h after 50 nM WJ460 treatment (Supplemental Fig. S5A). At 24 h, our results showed a significant increase of iron abundance in MiaPaCa-2, Panc-1 and PaTu 8988T cell lines while intracellular iron was not increased in BxPC-3 and HPNE cells (Fig. 4A). We then undertook rescue experiments with iron chelators, deferiprone (DFP) and deferoxamine (DFX). The DFP and DFX concentrations were chosen based on a concentration-response experiment (Supplemental Fig. S5B). The selected DFP and DFX concentrations (1 mM) were in accordance with previously reported ones [25]. In accordance with our previous results, 50 nM WJ460 for 24 h altered moderately MiaPaCa-2 cell growth while BxPC-3, Panc-1 and PaTu 8988T growth was reduced by 25–50% (Fig. 4B). Iron chelators restored significantly the growth in the BxPC-3, Panc-1 and PaTu 888T cell lines affected by WJ460. Despite a quantified increase in intracellular iron concentration and a successful rescue experiment using chelators, we were unable to determine the origin of the iron. Indeed, transferrin receptor (CD71), ferritin heavy chain, nuclear receptor coactivator (NCOA)-4 abundances were not significantly perturbated by WJ460 in Panc-1 cell line (Fig. 4C & Supplemental Fig. S5C). The growth rescue by iron chelators resulted probably from a consistent decrease of ROS accumulation (Fig. 4D). Additionally, we showed that Mdivi-1, a selective cell-permeable inhibitor of mitochondrial division and mitophagy, was able to prevent the WJ460-induced mitochondrial fragmentation (Supplemental Fig. S5D) and the ROS accumulation (Fig. 4D), suggesting that ROS accumulation was a consequence of free iron accumulation and mitophagy.

Fig. 3. WJ460 induces lipid peroxidation in PDAC cell lines.

(A–B) Malondialdehyde (MDA) concentration in PDAC (BxPC-3, MiaPaCa-2, Panc-1, PaTu 8988T) and pancreas normal epithelial (HPNE) cell lines exposed to 50 nM WJ460 for 24 h. Each data point represents mean ± SEM, n = 4. ***P < 0.001, **P < 0.01, *P < 0.05. (C) Trolox 5 mM mitigates the WJ460-induced reduction of cell confluency. Each data point represents mean ± SEM, n = 3. (D) Western-blot showing the x_c^- transporter SLC7A11, and glutathione peroxidase (GPX)-4 in PaTu 8988T and HPNE cells exposed to 50 nM WJ460 for 8–24 h. HSC70 was used as a loading control. Associated charts represent the relative abundance of SLC7A11 and GPX-4.

Fig. 4. WJ460 induces an iron-dependent cell death in PDAC cell lines.

(A) Intracellular iron concentration in PDAC (BxPC-3, MiaPaCa-2, Panc-1, PaTu 8988T) and pancreas normal epithelial (HPNE) cell lines exposed to 50 nM WJ460 for 24 h. Each data point represents mean ± SEM, n = 3. ****$P < 0.0001$, ***$P < 0.001$, *$P < 0.05$. (B) Treatment of PDAC cell lines with 50 nM WJ460 and iron chelators, 1 mM deperipone (DFP) or 1 mM deferoxamine (DFX). Each data point represents mean ± SEM, n = 3. (C) Western-blot showing the transferrin receptor CD71, heavy-chain ferritin, and nuclear receptor coactivator 4 (NCOA4) in Panc-1 cells exposed to 50 nM WJ460 for 8–24 h. HSC70 was used as a loading control. (D) Relative reactive oxygen species (ROS) accumulation in Panc-1 cell line treated for 24 h with 50 nM WJ460 and iron chelators, 1 mM DFP or 1 mM DFX, or mitophagy inhibitor 10 μM Mdivi-1. Each data point represents mean ± SEM, n = 3. ***$P < 0.001$, **$P < 0.01$, *$P < 0.05$.

3.5. WJ460 sensitizes Panc-1 cells to ferroptosis

We then decided to investigate the combination between WJ460 and drugs inducing ferroptosis, namely erastin (eradicator of Ras and ST-expressing cell) and RSL3 (Ras-selective lethality protein 3). First, we performed a drug titration curve in order to determine efficient concentration of each individual compound on Panc-1 cells. As previously described, 25 nM WJ460 was the lowest efficient concentration, but it poorly impaired cell growth (Fig. 5A). From one hand, erastin inhibited cell growth from 1 μM, and induced a 25% cell loss from 5 μM (Fig. 5B). On the other hand, RSL3 reduced cell growth from 25 nM, and 50 nM RSL3 induced a 25% cell loss (Fig. 5C). To test the synergy between WJ460 and erastin or RSL3, we combined several WJ460 concentrations (ranging from 10 to 50 nM) with several erastin (ranging from 1 to 50 μM) or RSL3 (ranging from 1 to 100 nM) and analyzed cell confluency. Kinetic analysis of relative confluency showed a strong reduction of cell growth with several drug combinations (Fig. 5D and E). Synergy analysis according to Chou-Talalay [21] showed several drug combinations with a combination index lower than 1, indicating synergy (Fig. 5F). The

more efficient combination were 25 nM WJ460/1 μM erastin (combination index = 0.415), 10 nM WJ460/10 μM erastin (combination index = 0.240), and 25 nM WJ460/1 nM RSL3 (combination index = 0.397).

4. Discussion

The mortality rate of PDAC is currently almost equal to its incidence and its 5-year survival rate is the lowest among all cancers. Unfortunately, projections do not predict an improvement since they suggest that it will be the second cause of death from cancer in less than 10 years [26]. This dismal reality is mainly due to a diagnosis at a very advanced stage of the disease and the relative lack of effectiveness of the available treatments. The development of new strategies and the identification of innovative therapeutic targets therefore remain priorities for this cancer.

As part of previous research aiming at identifying new biomarkers, our laboratory was among the first to describe the myoferlin as over-expressed in PDAC [1]. The expression of this protein correlates with a poor survival in PDAC patients [2,3], and we reported the inability of
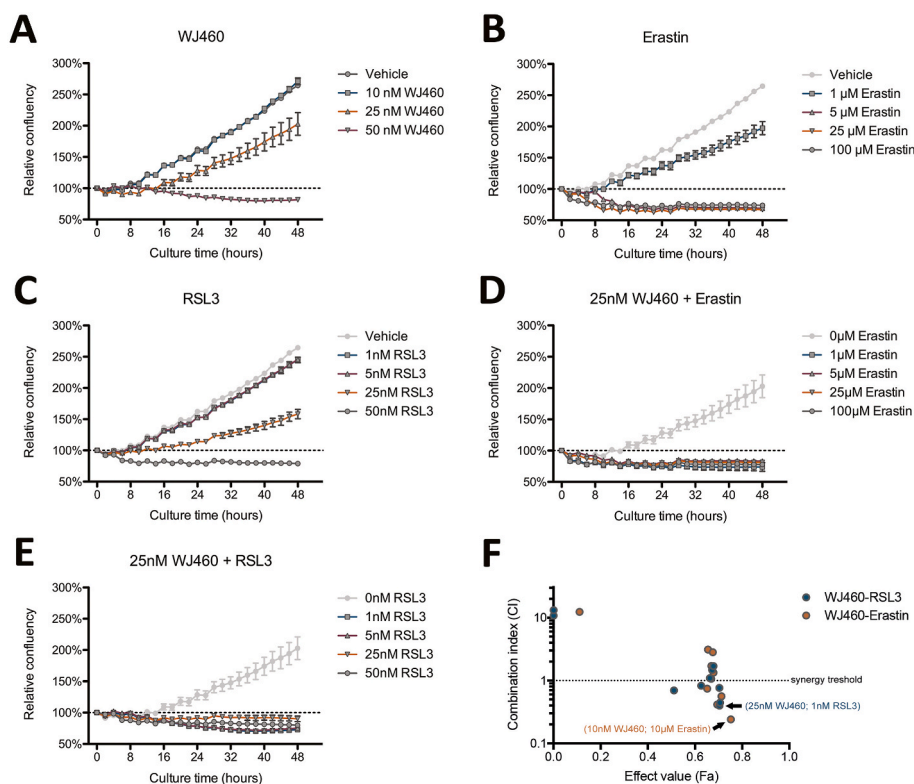
Fig. 5. WJ460 sensitizes Panc-1 cells to ferroptosis.
Cell growth inhibition of Panc-1 cells exposed for 48 h to (A) 10-50 nM WJ460, (B) 1-100 μM erastin, (C) 1-50 nM RSL3, (D) 25 nM WJ460 and 1-100 μM erastin, (E) 25 nM WJ460 and 1-50 nM RSL3. Each data point represents mean ± SEM, n = 3. (F) Combination index (CI) according to drug combination effect (Fa).

PDAC cells to migrate and implant in the liver when myoferlin expression is inhibited [27]. Recently, three innovative compounds have been described for their ability to bind to myoferlin and reduce the metastatic dissemination of breast [10], colon [12], and pancreas [11] cancers, demonstrating its pharmacopotential. In this study, we described that WJ460, a small compound binding to myoferlin, induced the same main biological effects as myoferlin gene silencing in several PDAC cell lines.

An important hallmark of cancers is their ability to evade from apoptosis [28]. Recently, ferroptosis was reported as an alternative regulated cell death triggered by a loss of antioxidant defense system [29]. Ferroptosis is relevant in the context of cancer because high iron levels support cancer proliferation, making cancer cells addicted to iron [30]. Therefore, important iron pools are naturally present within tumors. Interestingly, erastin and RSL3, two ferroptosis inducers, were reported to be particularly efficient in KRAS-mutated cancer cells [31]. As such, ferroptosis has been proposed as an alternative to treat patients with KRAS mutation. Our experiments revealed that WJ460 triggered an iron-dependent cell death with a negative modulation of the ferroptosis main regulators, SLC7A11 and GPX4, which physiologically protect cells from ROS and lipid peroxidation.

The labile iron pool may originate from different sources inside and/or outside the cell. First, ferritin can be degraded by autophagy with the help of NCOA4 driving ferritin to the lysosome and subsequent iron release [32]. Second, the iron uptake can be increased by an overexpression of the transferrin receptor leading to an overload of iron [31]. Finally, mitochondrial autophagy can participate to the labile iron pool increase by releasing iron from the numerous iron-sulfur clusters involved in oxidative phosphorylation [25]. In accordance with this alternative, our results indicate a mitophagy-dependent ROS accumulation, mainly in the cytosol. Myoferlin targeting results in an exacerbate mitophagy increasing lysosomal iron content from mitochondrial iron-sulfur clusters. The iron accumulation can be the cause of lysosomal membrane peroxidation and permeabilization [33] leading, in turn, to

lysosomal iron leakage [34]. Recent evidence demonstrates a lysosomal localization for myoferlin where it is essential to membrane protection [35]. According to this new function, myoferlin depletion should amplify the lysosomal membrane alteration and consequently the iron leakage. Interestingly, the iron leakage sustains a vicious cycle since it is both the cause and the consequence of the membrane alteration.

In the context of PDAC, only few reports described the priming of ferroptosis using gene silencing of metabolic enzyme [36] or inhibiting compounds [37]. In a single compound strategy, erastin is used at 20 μM to induce ferroptosis in Panc-1 cells [37,38]. We showed here that WJ460 was able to synergistically increase the efficiency of erastin and RSL3. Indeed, in combination with WJ460, 1 μM erastin or 1 nM RSL3 are potent enough to block Panc-1 cell growth. These compounds inhibit cell defenses against lipid peroxidation, respectively the x_c^- transporter and GPX4, and are potentiated by the ROS imbalance elicited by WJ460.

Our findings shed light on the biological effects of WJ460, a myoferlin-interacting compound. Targeting myoferlin either with this compound or by gene silencing produces similar effects, including ROS production and mitochondrial fission. We demonstrated that WJ460 cytotoxic effects were iron-dependent. Finally, we described a synergistic effect of WJ460 with erastin or RSL3 to induce ferroptosis. Consequently, targeting myoferlin may pave the way for new therapeutic combination. We propose to combine myoferlin targeting and low concentration of ferroptotic inducers to eradicate PDAC cells. In vivo experiments are still needed to validate the clinical potential of this combination.

Declaration of competing interest

Acknowledgments

Appendix A. Supplementary data

Supplementary data to this article can be found online at https://doi.org/10.1016/j.redox.2022.102324.

References

[1] A. Turtoi, D. Musmeci, Y. Wang, B. Dumont, J. Somja, G. Bevilacqua, E.D. Pauw, P. Delvenne, V. Castronovo, Identification of novel accessible proteins bearing diagnostic and therapeutic potential in human pancreatic ductal adenocarcinoma, J. Proteome Res. 10 (2011) 4302–4313, https://doi.org/10.1021/pr200527z.

[2] O. Peulen, G. Rademaker, S. Anania, A. Turtoi, A. Bellahcène, V. Castronovo, Ferlin overview: from membrane to cancer biology, Cells 8 (2019) 954, https://doi.org/10.3390/cells8090954.

[3] G. Rademaker, V. Hennequière, L. Brohée, M.-J. Nokin, F. Lovinfosse, S. Gofflot, J. Bellier, B. Costanza, M. Herfs, R. Peiffer, L. Bettendorff, C. Deroanne, M. Thiry, P. Delvenne, R. Hustinx, A. Bellahcène, V. Castronovo, O. Peulen, Myoferlin controls mitochondrial structure and activity in pancreatic ductal adenocarcinoma, and affects tumor aggressiveness, Oncogene 66 (2018) 1–15, https://doi.org/10.1038/s41388-018-0287-z.

[4] K. Fahmy, A. Gonzalez, M. Arafa, P. Peixoto, A. Bellahcène, A. Turtoi, P. Delvenne, M. Thiry, V. Castronovo, O. Peulen, Myoferlin plays a key role in VEGFA secretion and impacts tumor-associated angiogenesis in human pancreas cancer, Int. J. Cancer 138 (2016) 652–663, https://doi.org/10.1002/ijc.29820.

[5] A. Blomme, K. Fahmy, O. Peulen, B. Costanza, M. Fontaine, I. Struman, D. Baiwir, E.D. Pauw, M. Thiry, A. Bellahcène, V. Castronovo, A. Turtoi, Myoferlin is a novel exosomal protein and functional regulator of cancer-derived exosomes, Oncotarget 7 (2016) 83669–83683, https://doi.org/10.18632/oncotarget.13276.

[6] A. Blomme, B. Costanza, P. de Tullio, M. Thiry, G.V. Simaeys, S. Boutry, G. Doumont, E.D. Valentin, T. Hirano, T. Yokobori, S. Gofflot, O. Peulen, A. Bellahcène, F. Sherer, C.L. Goff, E. Cavalier, A. Mouithys-Mickalad, F. Jouret, P. G. Cusumano, E. Lifrange, R.N. Muller, S. Goldman, P. Delvenne, E.D. Pauw, M. Nishiyama, V. Castronovo, A. Turtoi, Myoferlin regulates cellular lipid metabolism and promotes metastases in triple-negative breast cancer, Oncogene 36 (2017) 2116–2130, https://doi.org/10.1038/onc.2016.369.

[7] G. Rademaker, B. Costanza, J. Bellier, M. Herfs, R. Peiffer, F. Agirman, N. Maloujahmoum, Y. Habraken, P. Delvenne, A. Bellahcène, V. Castronovo, O. Peulen, Human colon cancer cells highly express myoferlin to maintain a fit mitochondrial network and escape p53-driven apoptosis, Oncogenesis 8 (2019) 21, https://doi.org/10.1038/s41389-019-0130-6.

[8] S. Anania, R. Peiffer, R. Gilles, A. Hego, L. Deldicque, M. Francaux, A. Bellahcène, V. Castronovo, O. Peulen, Myoferlin is a yet unknown interactor of the mitochondrial dynamics' machinery in pancreas cancer cells, Cancers 12 (2020) 1643, https://doi.org/10.3390/cancers12061643.

[9] G.R. Anderson, S.E. Wardell, M. Cakir, C. Yip, Y. Ahn, M. Ali, A.P. Yllanes, C. A. Chao, D.P. McDonnell, K.C. Wood, Dysregulation of mitochondrial dynamics proteins are a targetable feature of human tumors, Nat. Commun. 9 (2018) 1677, https://doi.org/10.1038/s41467-018-04033-x.

[10] T. Zhang, L. Jingjie, Y. He, F. Yang, Y. Hao, W. Jin, J. Wu, Z. Sun, Y. Li, Y. Chen, Z. Yi, M. Liu, A small molecule targeting myoferlin exerts promising anti-tumor effects on breast cancer, Nat. Commun. 9 (2018) 3726, https://doi.org/10.1038/s41467-018-06179-0.

[11] Y. Li, Y. He, T. Shao, H. Pei, W. Guo, D. Mi, I. Krimm, Y. Zhang, P. Wang, X. Wang, M. Liu, Z. Yi, Y. Chen, Modification and biological evaluation of a series of 1,5-Diaryl-1,2,4-triazole compounds as novel agents against pancreatic cancer metastasis through targeting myoferlin, J. Med. Chem. 62 (2019) 4949–4966, https://doi.org/10.1021/acs.jmedchem.9b00059.

[12] Y. He, W. Kan, Y. Li, Y. Hao, A. Huang, H. Gu, M. Wang, Q. Wang, J. Chen, Z. Sun, M. Liu, Y. Chen, Z. Yi, A potent and selective small molecule inhibitor of myoferlin attenuates colorectal cancer progression, Clin. Transl. Med. 11 (2021) e289, https://doi.org/10.1002/ctm2.289.

[13] S.J. Dixon, K.M. Lemberg, M.R. Lamprecht, R. Skouta, E.M. Zaitsev, C.E. Gleason, D.N. Patel, A.J. Bauer, A.M. Cantley, W.S. Yang, B. Morrison, B.R. Stockwell, Ferroptosis: an iron-dependent form of nonapoptotic cell death, Cell 149 (2012) 1060–1072, https://doi.org/10.1016/j.cell.2012.03.042.

[14] M. Lo, V. Ling, Y.Z. Wang, P.W. Gout, The xc− cystine/glutamate antiporter: a mediator of pancreatic cancer growth with a role in drug resistance, Br. J. Cancer 99 (2008) 464–472, https://doi.org/10.1038/sj.bjc.6604485.

[15] M.A. Badgley, D.M. Kremer, H.C. Maurer, K.E. DelGiorno, H.-J. Lee, V. Purohit, I. R. Sagalovskiy, A. Ma, J. Kapilian, C.E.M. Firl, A.R. Decker, S.A. Sastra, C. F. Palermo, L.R. Andrade, P. Sajjakulnukit, L. Zhang, Z.P. Tolstyka, T. Hirschhorn, C. Lamb, T. Liu, W. Gu, E.S. Seeley, E. Stone, G. Georgiou, U. Manor, A. Iuga, G. M. Wahl, B.R. Stockwell, C.A. Lyssiotis, K.P. Olive, Cysteine depletion induces pancreatic tumor ferroptosis in mice, Science 368 (2020) 85–89, https://doi.org/10.1126/science.aaw9872.

[16] G. Sharbeen, J.A. McCarroll, A. Akerman, C. Kopecky, J. Youkhana, J. Kokkinos, J. Holst, C. Boyer, M. Erkan, D. Goldstein, P. Timpson, T.R. Cox, B.A. Pereira, J. L. Chitty, S.K. Fey, A.K. Najumudeen, A.D. Campbell, O.J. Sansom, R.M.C. Ignacio, S. Naim, J. Liu, N. Russia, J. Lee, A. Chou, A. Johns, A.J. Gill, E. Gonzales-Aloy, V. Gebski, Y.F. Guan, M. Pajic, N. Turner, M.V. Apte, T.P. Davis, J.P. Morton, K. S. Haghighi, J. Kasparian, B.J. McLean, Y.F.I. Setargew, A.P.C.G.I. Apgi, P. A. Phillips, Cancer-associated fibroblasts in pancreatic ductal adenocarcinoma determine response to SLC7A11 inhibition, Cancer Res. (2021), https://doi.org/10.1158/0008-5472.can-20-2496 canres.2496.2020.

[17] X. Yu, Y.C. Long, Crosstalk between cystine and glutathione is critical for the regulation of amino acid signaling pathways and ferroptosis, Sci. Rep. 6 (2016) 30033, https://doi.org/10.1038/srep30033.

[18] N. Matheus, S. Hansen, E. Rozet, E. Peixoto, E. Maquoi, V. Lambert, A. Noël, M. Frédérich, D. Mottet, P. de Tullio, An easy, convenient cell and tissue extraction protocol for nuclear magnetic resonance metabolomics, Phytochem Analysis 25 (2014) 342–349, https://doi.org/10.1002/pca.2498.

[19] J. Gao, B.A. Aksoy, U. Dogrusoz, G. Dresdner, B. Gross, S.O. Sumer, Y. Sun, A. Jacobsen, R. Sinha, E. Larsson, E. Cerami, C. Sander, N. Schultz, Integrative analysis of complex cancer genomics and clinical profiles using the cBioPortal, Sci. Signal. 6 (2013) pl1, https://doi.org/10.1126/scisignal.2004088.

[20] E. Cerami, J. Gao, U. Dogrusoz, B.E. Gross, S.O. Sumer, B.A. Aksoy, A. Jacobsen, C. J. Byrne, M.L. Heuer, E. Larsson, Y. Antipin, B. Reva, A.P. Goldberg, C. Sander, N. Schultz, The cBio Cancer Genomics Portal: an open platform for exploring multidimensional cancer genomics data, Cancer Discov. 2 (2012) 401–404, https://doi.org/10.1158/2159-8290.cd-12-0095.

[21] T.-C. Chou, Drug combination studies and their synergy quantification using the chou-talalay method, Cancer Res. 70 (2010) 440–446, https://doi.org/10.1158/0008-5472.can-09-1947.

[22] T.J. Humpton, B. Alagesan, G.M. DeNicola, D. Lu, G.N. Yordanov, C.S. Leonhardt, M.A. Yao, P. Alagesan, M.N. Zaatari, Y. Park, J.N. Skepper, K.F. Macleod, P. A. Perez-Mancera, M.P. Murphy, G.I. Evan, K.H. Vousden, D.A. Tuveson, Oncogenic Kras induces Nix-mediated mitophagy to promote pancreatic cancer, Cancer Discov. 9 (2019) 1268–1287, https://doi.org/10.1158/2159-8290.cd-18-1409.

[23] M. Gao, J. Yi, J. Zhu, A.M. Minikes, P. Monian, C.B. Thompson, X. Jiang, Role of mitochondria in ferroptosis, Mol Cell 73 (2019) 354–363, https://doi.org/10.1016/j.molcel.2018.10.042, e3.

[24] P. Koppula, Y. Zhang, J. Shi, W. Li, B. Gan, The glutamate/cystine antiporter SLC7A11/xCT enhances cancer cell dependency on glucose by exporting glutamate, J. Biol. Chem. 292 (2017) 14240–14249, https://doi.org/10.1074/jbc.m117.798405.

[25] G.F.G. Allen, R. Toth, J. James, I.G. Ganley, Loss of iron triggers PINK1/Parkin-independent mitophagy, EMBO Rep. 14 (2013) 1127–1135, https://doi.org/10.1038/embor.2013.168.

[26] L. Rahib, B.D. Smith, R. Aizenberg, A.B. Rosenzweig, J.M. Fleshman, L. M. Matrisian, Projecting cancer incidence and deaths to 2030: the unexpected burden of thyroid, liver, and pancreas cancers in the United States, Cancer Res. 74 (2014) 2913–2921, https://doi.org/10.1158/0008-5472.can-14-0155.

[27] G. Rademaker, B. Costanza, S. Anania, F. Agirman, N. Maloujahmoum, E. D. Valentin, J.J. Goval, A. Bellahcène, V. Castronovo, O. Peulen, Myoferlin contributes to the metastatic phenotype of pancreatic cancer cells by enhancing their migratory capacity through the control of oxidative phosphorylation, Cancers 11 (2019) 853, https://doi.org/10.3390/cancers11060853.

[28] D. Hanahan, R.A. Weinberg, Hallmarks of cancer: the next generation, Cell 144 (2011) 646–674, https://doi.org/10.1016/j.cell.2011.02.013.

[29] S.J. Dixon, B.R. Stockwell, The hallmarks of ferroptosis, Annu. Rev. Cell Biol. 3 (2019) 35–54, https://doi.org/10.1146/annurev-cancerbio-030518-055844.

[30] S. Toyokuni, Role of iron in carcinogenesis: cancer as a ferrotoxic disease, Cancer Sci. 100 (2009) 9–16, https://doi.org/10.1111/j.1349-7006.2008.01001.x.

[31] T. Hirschhorn, B.R. Stockwell, The development of the concept of ferroptosis, Free Radic. Biol. Med. 133 (2019) 130–143, https://doi.org/10.1016/j.freeradbiomed.2018.09.043.

[32] J.D. Mancias, X. Wang, S.P. Gygi, J.W. Harper, A.C. Kimmelman, Quantitative proteomics identifies NCOA4 as the cargo receptor mediating ferritinophagy, Nature 509 (2014) 105–109, https://doi.org/10.1038/nature13148.

[33] Y. Lin, D.L. Epstein, P.B. Liton, Intralysosomal iron induces lysosomal membrane permeabilization and cathepsin D–mediated cell death in trabecular meshwork cells exposed to oxidative stress, Invest Opthalmol Vis Sci 51 (2010) 6483, https://doi.org/10.1167/iovs.10-5410.

[34] T. Kurz, A. Terman, B. Gustafsson, U.T. Brunk, Lysosomes in iron metabolism, ageing and apoptosis, Histochem. Cell Biol. 129 (2008) 389–406, https://doi.org/10.1007/s00418-008-0394-y.

[35] S. Gupta, J. Yano, V. Mercier, H.H. Htwe, H.R. Shin, G. Rademaker, Z. Cakir, T. Ituarte, K.W. Wen, G.E. Kim, R. Zoncu, A. Roux, D.W. Dawson, R.M. Perera,

Lysosomal retargeting of Myoferlin mitigates membrane stress to enable pancreatic cancer growth, Nat. Cell Biol. 23 (2021) 232–242, https://doi.org/10.1038/s41556-021-00644-7.

[36] D.M. Kremer, B.S. Nelson, L. Lin, E.L. Yarosz, C.J. Halbrook, S.A. Kerk, P. Sajjakulnukit, A. Myers, G. Thurston, S.W. Hou, E.S. Carpenter, A.C. Andren, Z. C. Nwosu, N. Cusmano, S. Wisner, N.E. Mbah, M. Shan, N.K. Das, B. Magnuson, A. C. Little, M.R. Savani, J. Ramos, T. Gao, S.A. Sastra, C.F. Palermo, M.A. Badgley, L. Zhang, J.M. Asara, S.K. McBrayer, M.P. di Magliano, H.C. Crawford, Y.M. Shah, K.P. Olive, C.A. Lyssiotis, GOT1 inhibition promotes pancreatic cancer cell death

by ferroptosis, Nat. Commun. 12 (2021) 4860, https://doi.org/10.1038/s41467-021-24859-2.

[37] B.C. Yang, P.S. Leung, Irisin is a positive regulator for ferroptosis in pancreatic cancer, Mol Ther - Oncolytics 18 (2020) 457–466, https://doi.org/10.1016/j.omto.2020.08.002.

[38] S. Zhu, Q. Zhang, X. Sun, H.J. Zeh, M.T. Lotze, R. Kang, D. Tang, HSPA5 regulates ferroptotic cell death in cancer cells, Cancer Res. 77 (2017) 2064–2077, https://doi.org/10.1158/0008-5472.can-16-1979.